Parameterizing non-propagating form drag over rough bathymetry

Jody M. Klymak *

University of Victoria, Victoria, BC, Canada

Dhruv Balwada

University of Washington, Seattle, WA, USA

Alberto Naveira Garabato

University of Souathampton, National Oceanography Centre, Southampton, United Kingdom

Ryan Abernathy

Columbia University, New York, New York, USA

ABSTRACT

Slowly-evolving stratified mean and eddying flow over rough topography is subject to substantial drag due to the internal motions generated, but often numerical simulations are carried out at resolutions where this "wave" drag must be parameterized. Here we propose a simple parameterization of this drag that has a minimum of fit parameters compared to existing schemes. The parameterization smoothly transitions from a quadratic drag law ($\sim h u_0^2$) for low-Nh/u_0 (linear wave dynamics) regimes to a linear drag law ($\sim h^2 u_0 N$) for high-Nh/u_0 flows (blocking and hydraulic dynamics), where N is the stratification, h is the amplitude of the topography, and u_0 is the near-bottom velocity; the parameterization does not have a dependence on Coriolis frequency. Simulations carried out in a channel with synthetic bathymetry and steady body forcing indicate that this parameterization accurately predicts drag across a broad range of forcing parameters. The parameterization is also tested in more realistic simulations of wind-driven channel flows that generate mesoscale eddy fields, a setup where the mean downstream transport is very sensitive to the bottom drag parameterization and its effect on the eddies. In these simulations, the parameterization is found to replicate the effect of rough bathymetry both on the eddies and the mean flow, but the value of h must be doubled over the value used in the steady simulations for optimal agreement.

1. Introduction

Stratified flows passing over bathymetry experience drags that are often many orders of magnitude larger than that effected by skin friction alone, due to the creation of internal motions that either radiate away as internal waves (Bell 1975) or are trapped as "non-propagating" motions near the topography (i.e. Bacmeister and Pierrehumbert 1988). Including these motions in large-scale models is important to the momentum balance and mixing in both the ocean and the atmosphere, so they must be parameterized if simulations do not include enough resolution to capture the small-scale topography.

Here we consider low-frequency flows, where the variation in the flow is taken to be substantially sub-inertial and has a given near-bottom speed u_0. The flow is taken to be over idealized topography that is stochastically specified by empirical models

in the form given by Goff and Arbic (2010), rather than over any sort of realistic topography. In this situation, there are two simple parameters controlling the flow regimes found. First, for the high-horizontal wavenumber (k) part of the topography where $u_0 k > f$, radiating internal lee waves are possible because the intrinsic frequency is greater than f. If the second parameter $Nh/u_o \lesssim \pi$, where N is the near-topography stratification and h is the amplitude of the topography, then linear theory applies and the drag on the mean flow can be analytically calculated (Bell 1975). The high-wavenumber part of the topography typically has a small amplitude (so-called "abyssal hills"), so the flows are well-approximated by linear theory (Nikurashin and Ferrari 2010; Nikurashin et al. 2014). The radiated waves interact via wave-wave interactions to cause a halo of turbulence in a region near the sea floor that is a few hundred meters deep, and amenable to prediction by weakly non-linear theory (Polzin 2009). Substantial recent work indicates that pa-

---

* *Corresponding author*: Jody Klymak, jklymak@uvic.ca, University of Victoria, Victoria, BC, Canada

rameterizing the "abyssal hills" can alter the large-scale circulation and stratification (Melet et al. 2013; de Lavergne et al. 2017, i.e.).

For larger-scale topography ($u_0 k < f$) the internal motions cannot radiate as internal waves and, in the linear limit, only remove energy when the flow changes as an evanescent response is set up, and hence this drag is termed "non-propagating". However, the topographic spectra are typically red, and hence the amplitudes h appropriate at these scales tend to be substantially larger than for high-wavenumber topography, and Nh/u_0 can become quite large. The flow at this scale is thus inherently non-linear, and there is substantial local blocking upstream of topographic features, and breaking downstream. For the oceanic situation, Klymak (2018) demonstrates that for a typical bathymetric spectrum (i.e. the ones used by Nikurashin et al. 2014) the large-scale bathymetry was responsible for 2/3 of the total dissipation in the flow, and hence is crucial to include in parameterizations.

The importance of parameterizing drag and turbulence due to non-propagating motions over and around large-amplitude topography ($Nh/u_0 >> 1$) has been long realized by the atmospheric science community, and the enhanced mountain drag is imperative to properly simulate the atmosphere (i.e. Bacmeister and Pierrehumbert 1988; Lott and Miller 1997). A number of schemes have been devised based on the fact that substantial portions of the flow can be blocked around an isolated obstacle, and hence the drag becomes quadratic with the flow speed, and proportional to the cross-sectional area of the obstacle exposed to the mean flow (i.e. Scinocca and McFarlane 2000; Garner 2005). These parameterized drags have been shown to be important in numerical simulations of the ocean (Trossman et al. 2013, 2016), and to have promise when compared to observations (Trossman et al. 2015). These parameterizations are quadratic in flow speed and linear in obstacle height corrected by the blocking depth $h_b = u_0/N$, i.e.

$$D_{np} \sim (h - h_b)\, u_0\, |u_0|. \qquad (1)$$

Conversely, (Klymak et al. 2010) found that drag for $Nh/u_0 >> 1$ is linear in u_0 and quadratic in height for a two-dimensional obstacle:

$$\frac{D_{np}}{\rho_0} \approx \frac{u_0^2 h}{L} \frac{\pi}{2} \left[\frac{Nh}{u_0} + \pi \right] = C_l u_0 + C_q u_0^2, \qquad (2)$$

where L is an along-flow lateral scale (discussed below), and we have defined a linear drag co-efficient as $C_l = \frac{Nh^2\pi}{2L}$ and a quadratic drag co-efficient as $C_q = \frac{h\pi^2}{2L}$. Note that the quadratic term has the

same scaling as the non-linear drag typically used in the atmosphere for low Nh/u_0.

The goal of this paper is to test the appropriateness of the parameterization in equation (2), and argue that it provides an accurate yet simple way to transition between high- and low-Nh/u_0 flow regimes with a minimum of fit parameters. It was shown in Klymak (2018) that the non-propagating drag is indeed linear in the flow speed u_0, and not quadratic. Here we test the rest of the parameterization both via idealized simulations that also vary N, h and the Coriolis parameter f, and via more realistic, but still idealized, wind- and thermally forced channel flows. After specifying the numerics used in the simulations (section 2), we argue that equation (2) is indeed appropriate across a large range of parameters (section 3). The paper subsequently considers a large number of simulations that are idealizations of the flow in the Southern Ocean (section 4). The wind-driven channel was chosen for testing the parameterization because it is a closed system that still demonstrates substantial complexity that may be met by an eddy-resolving, large-scale simulation, and there is substantial literature that uses it already (i.e. Abernathey and Cessi 2014; Marshall et al. 2017).

2. Model configurations

Two types of simulation are used in this paper. The first is a doubly-periodic domain forced with a cross-channel body force that, absent other forces, is geostrophically balanced by an along-channel flow. Stratification, topographic roughness and Coriolis frequency are varied to test the parameterization of the near-bottom drag. The second configuration is a long re-entrant channel that has a large Gaussian ridge in the middle and varying roughness. This model is forced with a wind stress and thermal relaxation at the surface, and the bottom drag is either resolved or parameterized.

The `MITgcm` was used for all simulations (Marshall et al. 1997), in a manner analogous to previous work at similar scales (Buijsman et al. 2014; Klymak et al. 2016; Klymak 2018). Background explicit vertical and horizontal viscosity and diffusivity are kept low ($K_\rho = \nu = 10^{-5}$ m^2 s^{-1}) except in the presence of resolved density overturns, where the vertical viscosity and diffusions are increased in a manner consistent with the expected Thorpe scale (Klymak and Legg 2010). There is also numerical diffusivity and dissipation due to the second-order flux-limiting temperature advection scheme (`tempAdvScheme=77`; see the MITgcm manual). Using a weak explicit diffusivity allows the internal wave field to evolve freely to the extent that the chosen resolution allows,

rather than adding artificial damping (Shakespeare and Hogg 2017). For the work carried out here, the terms in the energy budget are all calculated and the residual is identified as the dissipation. However, the spatial distribution of explicit dissipation (calculated from the explicit viscosities and local shears) is similar to the spatial distribution of the residual of the energy budget. The model is run in hydrostatic mode for all simulations.

a. Doubly periodic, idealized forcing

These simulations are identical to those used in Klymak (2018), and inspired by Nikurashin et al. (2014). We assume a doubly periodic domain with constant stratification and a mean flow in the x-direction forced over rough topography. The strength of the flow maintained by a body force meant to simulate an externally-imposed surface pressure gradient. The doubly periodic lateral domain of 409.6 km in the x direction and 118.4 km in the y direction is chosen to capture sufficient variance in the large-scale topography. All simulations had a vertical resolution of 10 m over 4000 m depth. 1-km scale runs were spun up for 200 h.

The topography is the low-passed version of that used in Klymak (2018) with parameters given by:

$$P_{2D}(k,l) = \frac{2\pi h^2 (\mu - 2)}{k_0 l_0} \left(1 + \frac{k^2}{k_0^2} + \frac{l^2}{l_0^2}\right)^{-\mu/2}, \quad (3)$$

where h is the root-mean-square of the topographic height, $\mu = 3.5$ is a parameter setting the high-wavenumber slope of -1.75, and $k_0 = l_0 = 1.8 \times 10^{-4}$ rad m^{-1} are parameters that set the wavelength at which the spectrum of the topography starts to flatten out toward a white low-wavenumber spectrum. A range of values were tested for h, the background stratification N, k_0, and f.

b. Wind-forced channel simulations

The second set of simulations are run in a zonal channel forced by a sinusoidal wind stress and temperature relaxation at the surface. The wind-forced domain has the same numerics as the simulations above. The channel is 1024 km wide and 1600 km long (FIG. 1). The bathymetry is 3000 m deep, with sloping walls along the north and south wall faces, and a Gaussian ridge in the middle of the domain with a lateral scale of 100 km and a height of 1000 m, so that the shallowest point on the ridge is at 2000 m depth. Simulations are run with smooth seafloor bathymetries, and bathymetries with an added roughness that follows the same statistics as in the previous section (FIG. 2). These runs are started

with a uniform temperature of 4°C, and the temperature is forced at the surface with a relaxation time scale of 48 hours to be 4°C at the southern end, and linearly increasing to 12°C at the northern end. A sinusoidally-varying wind forcing is also applied down-channel, with a peak in the center of the channel of 0.2 Pa m^{-2}, and nulls at the north and south walls. This forcing and setup are meant to emulate many wind-driven channel studies (i.e. Abernathey and Cessi 2014; Marshall et al. 2017).
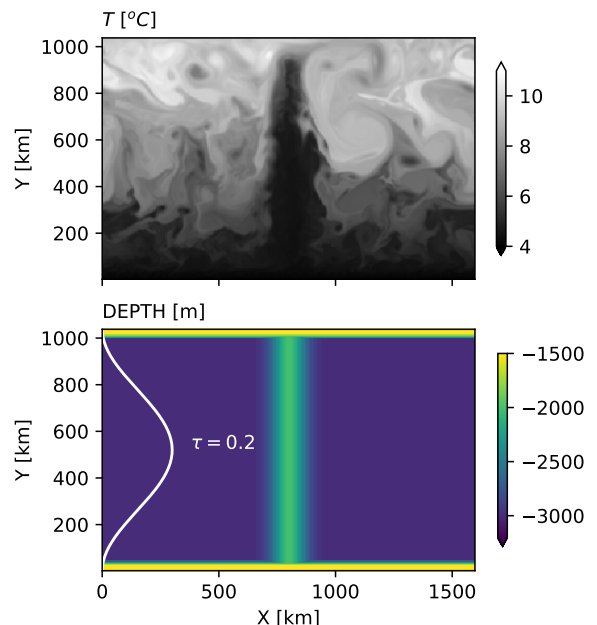

FIG. 1. Wind forced channel configuration.

These simulations were run in stages; a 20-km horizontal resolution and 80-m vertical resolution simulation was run for 100 years with the smooth bathymetry. A second run was made with the lateral resolution increased to 5 km, and the vertical resolution increased to 40 m, for 10 years. 5 km was the limit of what we could feasible simulate at a manageable computing cost, and the indication from Klymak (2018) is that this resolution will provide a drag in flows with rough bathymetry that is probably exaggerated by a factor of 1.4 compared to simulations with respective horizontal and vertical resolutions of 100 m and 10 m. As noted below, the simulations are close to being in mechanical equilibrium, but they are not anywhere near thermal equilibrium, which would require several centuries of simulation (i.e. Munday et al. 2015, run similar simulations for 620 years).
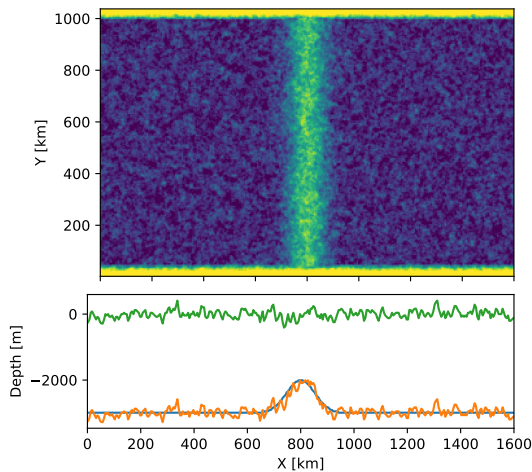
FIG. 2. Wind-forced channel bathymetry, with stochastic roughness added.

3. Parameterizing drag due to large-horizontal-scale topography

The first series of simulations were run with a body force over doubly-periodic stochastic topography similar to Klymak (2018), where here we only consider topography low-passed in space so that variance at horizontal scales smaller than 6 km is attenuated. At smaller scales, linear lee-wave parameterizations tend to do well, so we are only interested in parameterizing the large scales here. For comparison with the parameterization (equation (2)), we choose a representative horizontal spacing between obstacles of $L = (100 \text{ km}) 1.8 \times 10^{-4} \text{ rad m}^{-1}/k_0$, where k_0 is the roll-off wavenumber of the topographic spectrum (Klymak 2018). Simulations were run with a base configuration of $f = 10^{-4} \text{ rad s}^{-1}$, $u_0 = 0.1 \text{ m s}^{-1}$, $N = 10^{-3} \text{ rad s}^{-1}$, a maximum depth $H = 4000$ m, and a topographic roughness on top of this as described by equation (3) with a basic amplitude of $h = 305$ m and $k_0 = l_0 = 1.8 \times 10^{-4} \text{ rad m}^{-1}$. Energy budgets were performed on the runs, as described in (Klymak 2018), and an average vertically integrated dissipation rate across the domain was computed as the integral of vF_b, where F_b is the y-direction body force used to force the model, and v the north-south velocity.

Simulations were then carried out as deviations from the base values. First, h was varied, with $h = 155$, 305 and 610 m (FIG. 3a); we find that higher obstacles lead to more dissipation. The scaling is steeper with h than linear, and there appears to be some curvature to the response with h, as predicted. We are prevented from exploring smaller-scale topography by the vertical resolution of the model setup.

As the length scale L is changed by varying k_0 (FIG. 3b), we see that there is less dissipation with increasing length scale as expected, though the dissipation appears to plateau as the obstacles get closer together. This is likely because the peaks become close to a Rossby radius apart, and the topographic elements become less distinct.

As stratification is increased, $N = 0.5$, 2, 4 $\times 10^{-3} \text{ rad s}^{-1}$ (FIG. 3c), we see that dissipation goes up, as predicted. This is the starkest difference with the non-propagating drag parameterizations used in previous literature, which do not account for stratification. These simulations show that for larger values of Nh/u_0, the stratification plays a leading-order role.

There appears to be, at most, a weak dependence on the Coriolis force (FIG. 3d), again as predicted by equation (2) where there is no dependence on the Coriolis parameter. The agreement is not perfect; there is a 30% drop in dissipation as the Coriolis parameter drops to the value that corresponds to 15 N. However here we have again not changed the topography, so as f drops more internal waves are able to radiate rather than being blocked, a complication we have not tried to account for.

Finally, Klymak (2018) showed a clear dependence on u_o that follows that predicted by equation (2), so we do not reproduce that here.

Overall, the parameterization appears to do well over a wide range of ocean-relevant conditions. It has the advantages over other schemes of its containing only one ad-hoc parameter, and its allowance of a seamless merging of the parameterizations for high- and low-Nh/u_0 flows without arbitrary cut-off parameters. Conversely, the parameterization does not include the high-wavenumber component of the topography, and hence misses the internal wave dissipation, but again, there have been robust attempts at addressing that portion of the drag problem already (Nikurashin et al. 2014).

4. Wind-forced channel parameterization

The doubly periodic simulations forced via a body force are not very applicable to the abyssal ocean, where mean flows tend to be dominated by eddying motions with sub-inertial time scales. Thus we here test our parameterization in a wind- and thermally driven simulation that is just forced at the surface, allowing the near-bottom drag to evolve on its own, and buoyancy to be replenished by the overturning circulation in the channel. The simulation chosen was a wind-forced re-entrant channel with relaxation of the surface temperature to a north-south gradient, and a large-scale Gaussian ridge in the middle of the
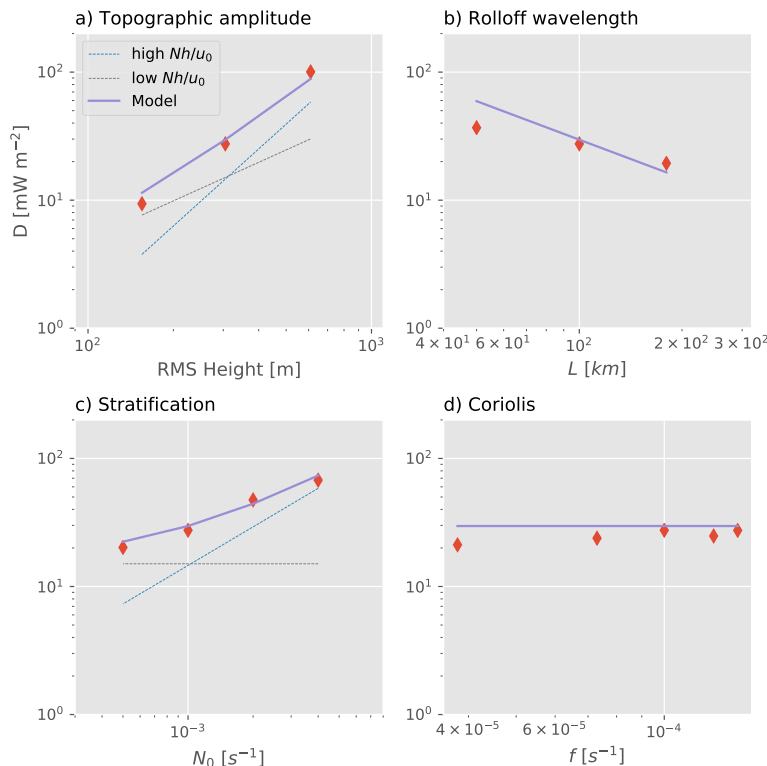
FIG. 3. Dependence of simulations on varying a) stochastic topographic amplitude; b) the roll-off wavelength at which the topographic amplitude starts to fall off; c) the stratification, and d) the Coriolis parameter. In each panel, the expectation from the model given by equation (2) is indicated, with both the high- and low-Nh/U asymptotes shown as thin dashed lines.

channel. This style of simulation catalyzes eddies in the flow (Abernathey and Cessi 2014), and has been shown to be very sensitive to the parameterization of the bottom drag (Marshall et al. 2017).

Simulations were made that had roughness down to the 6-km horizontal scale, and these were compared to simulations that had the drag due to that roughness parameterized using equation (2). As noted above, a smooth version of the model was run for 100 years at 20-km horizontal resolution, and then at 5 km for 10 years. The expectation, following Marshall et al. (2017), is that the rougher bathymetry, and simulations where the roughness is parameterized, will have faster spin-down of the eddies, more baroclinicity, and hence stronger downstream transport.

The smooth-bathymetry simulation was run with either a weak quadratic bottom drag ($C_q = 10^{-3}$), or with a bottom drag based on the parameterization above (equation (2)), meant to simulate the drag effect of the rough bathymetry. This was implemented as a quadratic plus linear drag in the model, using an approximate near-bottom stratification of

$N \approx 5 \times 10^{-4}$ rad/s, a topographic amplitude of $h_0 = 305$ m, and a lateral scale of 100 km, yielding for the base run a linear coefficient of $C_l = 7.3 \times 10^{-4}$ and a quadratic coefficient of $C_q = 1.5 \times 10^{-2}$. A better parameterization would be to make the coefficients depend on the observed near-bottom stratification, rather than choosing a value for N; however, that complexity was not addressed in these simulations.

A second important change was made to these simulations. Typically, the linear and quadratic drags are applied at the bottom-most cell of the model. However this leads to excessive near-bottom shear, and does not slow the water down over the range of depths that it does in the simulations with rough bathymetry. In order to simulate this effect, the bottom drag is evenly distributed over the bottom 7 grid cells, or over a vertical scale of about 280 m, similar to the vertical blocking scale of the topography $\pi u_0/N$ (Klymak et al. 2010). This is analogous to what was done by Trossman et al. (2016), who applied their non-propagating drag over the bottom 500 m.
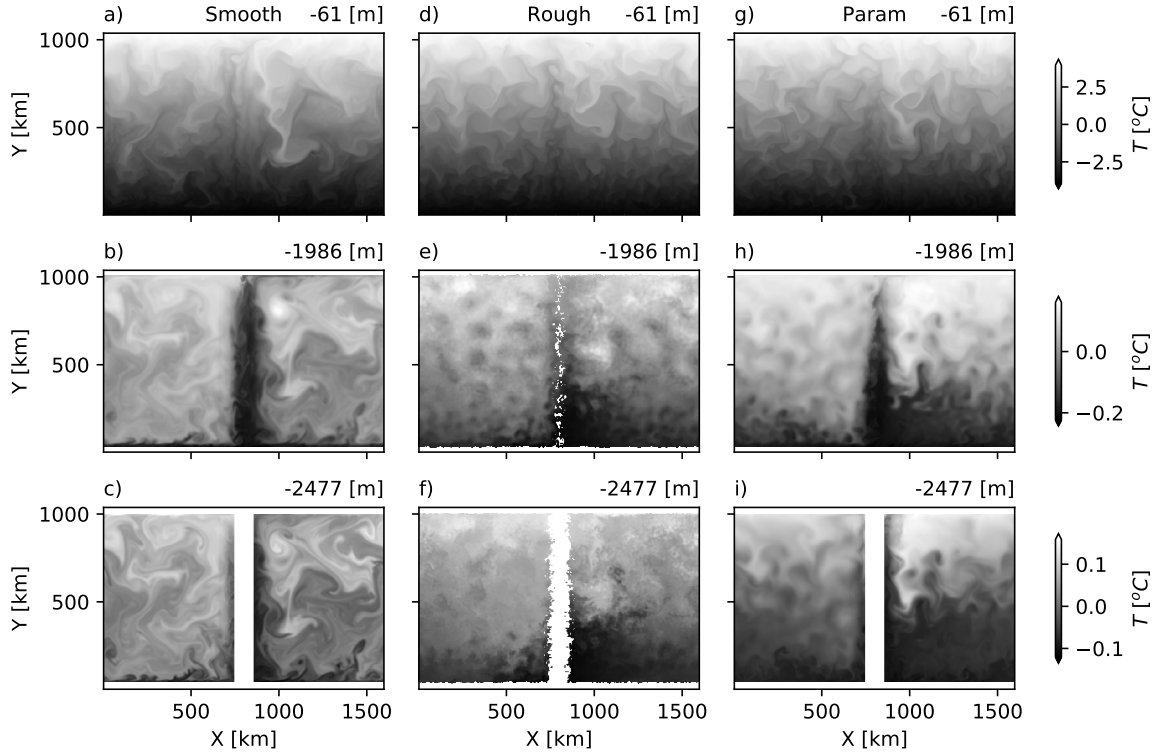
FIG. 4. Example lateral temperature slices (as anomalies from the mean at that depth) through the simulations at depths of -61 m, -1986 m, and -2477 m, with SMOOTH bathymetry in the first column, a synthetic ROUGH bathymetry in the second column, and an enhanced parameterized drag in the third column.

a. Flow response

Example lateral slices of temperature through the simulations show similar features between the SMOOTH and ROUGH simulations (FIG. 4), but small-scales are suppressed in the ROUGH simulation leading to a more ordered eddy field near the surface as the cascade to small scales is hampered. The PARAM simulation has similarly suppressed eddy filamentation. Note that all three simulations have different mean temperatures at these depths, a symptom of the fact that none of the runs are in thermal equilibrium.

Spectra of vertical velocity (FIG. 5) clearly show the suppression of eddies at subinertial frequencies in the ROUGH and PARAM simulations. Note the relatively weak internal wave field in all three simulations, which is unsurprising because any trapped internal waves would be subinertial in the Eulerian frame of reference, and the usual sources of propagating internal wave energy are missing.

The effect on the large-scale flow is as predicted by other studies (i.e. Marshall et al. 2017). Suppressing the mesoscale eddy field increases the baro-clinicity of the flow significantly, as well as deepening the thermocline (FIG. 6). The reason for this is that eddies are necessary to transmit surface stress down through the water column to ultimately be removed at the bottom. If the eddies are spun down more quickly, the flow must develop more baroclinicity, and hence more baroclinic instabilities, until a sufficiently large eddy stress exists to allow the flow to come into steady state. A byproduct is that there will be a stronger near-surface flow, and an increase in the transport along the channel (see below).

An interesting effect of the rough bathymetry (and its parameterization) is to greatly alter the standing meander that forms directly downstream of the basin-scale Gaussian ridge, most clearly seen by looking at the bottom pressure signal (FIG. 7). There is low pressure over the ridge in all three simulations, but downstream the large anticyclone is not as strong in the ROUGH and PARAM simulations. The effect of this on the large-scale drag is beyond our scope here, but is a curious result of adding more friction to the bottom drag (Thompson and Naveira Garabato 2014, e.g.).
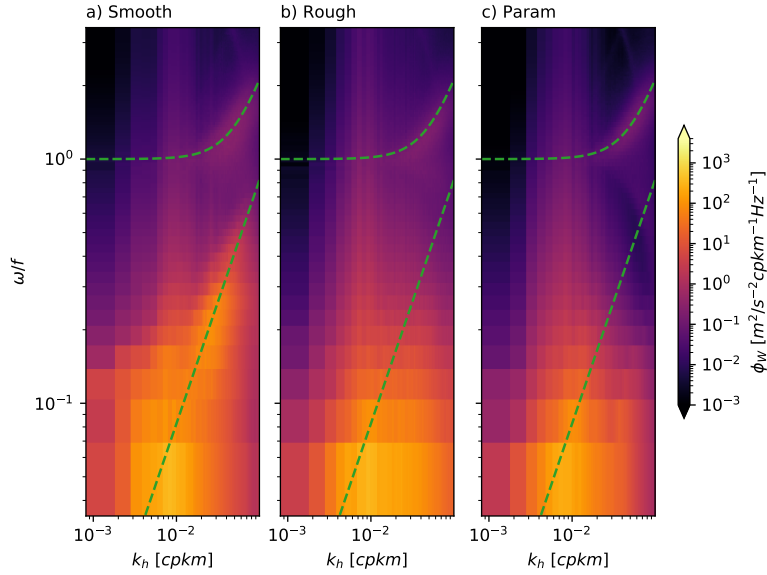
FIG. 5. Two-dimensional spectra of vertical kinetic energy at -1986 m for the three main simulations. The dashed green lines are a mode-1 internal wave dispersion relation (at super-inertial frequencies) and eddy motion assuming eddy propagation speeds of 8 km/d.

b. Integrated response and parameterization

The overall effect of the rough topography and its parameterization is to lead to smaller eddy kinetic energy by approximately 50% (FIG. 8a), and stronger downstream transport by up to a factor of four (FIG. 8c). The time series also make it clear that the simulations are in approximate mechanical steady state (FIG. 8a), but that they have not reached thermal equilibrium (FIG. 8b), which would take a few hundred years of simulation.

Parameterizing the drag due to the rough bathymetry was attempted in a few different ways. First, we tried a run with just a quadratic drag coefficient of $C_Q = 0.05$, and a separate run with just a linear drag coefficient of $C_L = 0.0025$. These are quite high drag coefficients, and lead to a strong increase of the down-channel transport (FIG. 8c), to 35 and 30 Sv respectively. Our first attempt to parameterize the rough drag was in equation (2) with $h = 305$ m as the amplitude of the bathymetry in the ROUGH simulations. This direct use of the parameterization proposed above meant adopting $C_l = 7.3 \times 10^{-4}$ and $C_q = 1.5 \times 10^{-2}$ (PARAM), but leads to a downstream transport that is too weak (FIG. 8c, green curve). An ad-hoc doubling of the "effective" value of h in the parameterization to 610 m leads to a much closer fit to the downstream transport (DOUBLE, FIG. 8c, red curve).

In these simulations, it is easiest to change the topographic amplitude, so we have done so over a range of topographic heights that are relatively large, 305 m (the cases shown above), 450 m, and 610 m. We ran the model with explicit rough bathymetry, and with parameterized drags. For the linear-only drag law we increased the coefficient by the square of the topographic height, and for the quadratic-only drag law we increased the coefficient linearly with the topographic height. For the combined drag as proposed in this paper, we ran the model with both h and $2h$.

As the stochastic topographic amplitude h is increased in the model simulations with explicit roughness, the downstream transport increases from 45 Sv to 62 Sv (FIG. 9, orange), due to the extra suppression of eddies. The quadratic form drag is assumed to scale with h, and hence does not see as much of an enhancement in downstream transport as h is increased (FIG. 9, gray, dashed). The linear form drag scales as h^2, and has a larger fractional increase in the downstream transport than is observed (FIG. 9, gray, dash-dot). The parameterization (FIG. 9, green curve), and the version with DOUBLE the topographic amplitude ((FIG. 9, red curve), have dependence on h that is very similar to the explicit bathymetry simulation. The DOUBLE drag law with $2h$ also has the correct amplitudes. Of course, both the linear or quadratic drags could have been tuned to better match the rough bathymetry simulations for any
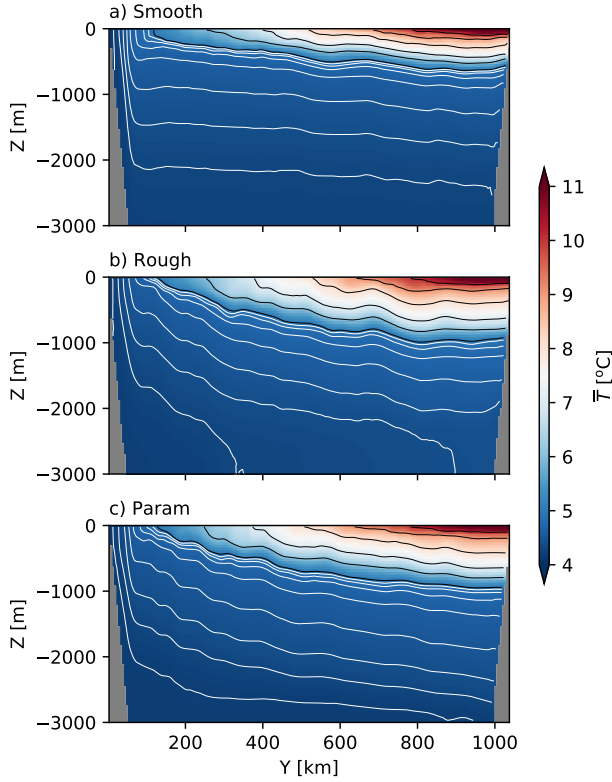
Fɪɢ. 6. Zonal temperature sections, averaged from x=0 to 500 km. Black contours are every degree C, white contours every 1/10 degree C from 5 to 4 degrees for three simulations a) Sᴍᴏᴏᴛʜ bathymetry, b) Rᴏᴜɢʜ bathymetry and c) smooth bathymetry with the "double-h" parameterization.

particular value of h, but the point is that the dependence on other values of h would still be incorrect, such that the hybrid scheme is an improvement over both.
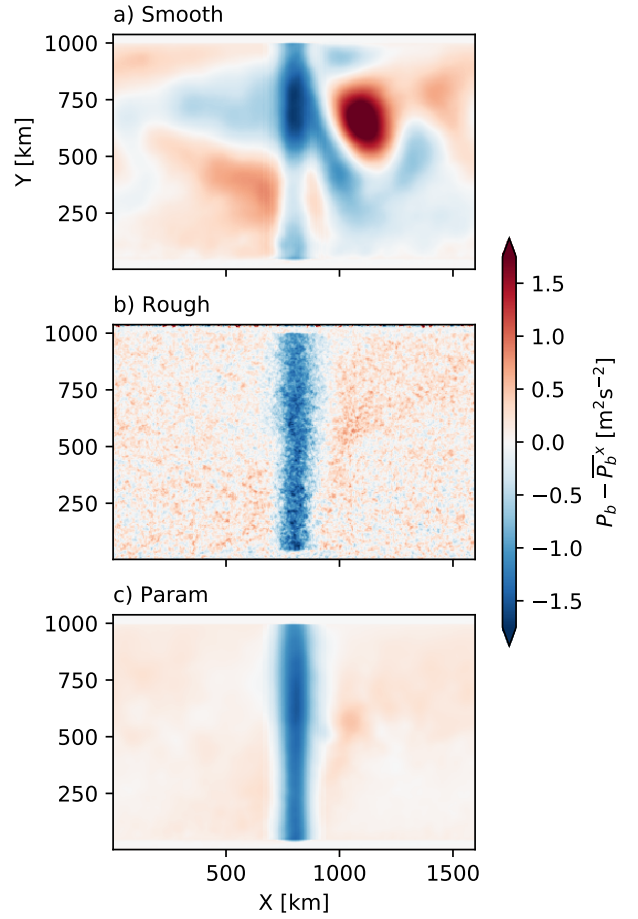

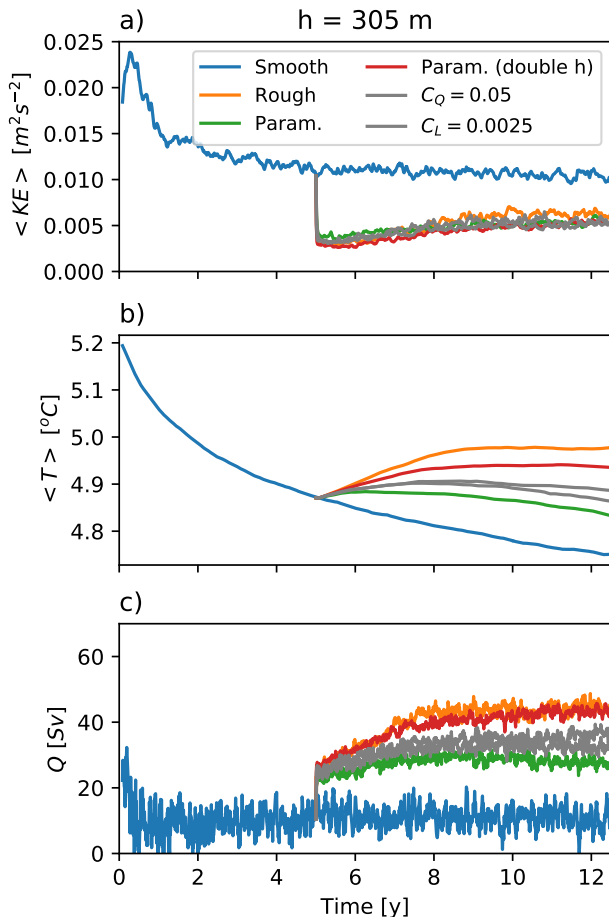Fɪɢ. 7. Bottom pressure averaged over last two years of the simulation with the zonal means removed.

FIG. 8. a) Model-mean kinetic energy in the simulations with various parameterizations of the drag. b) Model-mean temperature c) Mean downstream transport. SMOOTH is with no roughness and weak quadratic drag, ROUGH has stochastic bathymetry in the model, PARAM is smooth bathymetry with a hybrid linear/quadratic parameterization given in equation (2), and the red curve is with the same parameterization but h doubled. C_Q is with a heightened quadratic drag only, and C_L is with a heightened linear drag only.
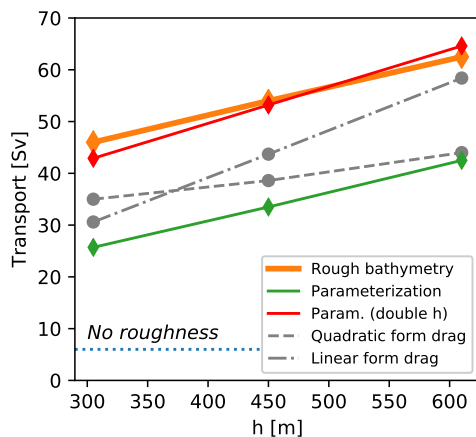

FIG. 9. Effects on the downstream transport of different roughness parameterizations. "Rough" is the 5-km simulations with resolved topography included. "Parameterization" is the parameterization suggested in this paper. "Param. (double h)" (red) is the same parameterization, but with the topographic height doubled in the parameterization (i.e. peak-to-trough height). Simulations with a quadratic (in velocity) form drag (grey dashed) and linear (in velocity) form drag only, roughly scaled to match the ROUGH simulations.

5. Discussion

Using the hybrid drag parameterization, equation (2), improves the simulation of bottom roughness as quantified by the downstream transport in the idealized wind-driven channel compared to runs with a linear or quadratic drag only. There are a few straight-forward caveats to this finding that should be noted. First, the body-forced runs (no wind forcing) found that the parameterization should use the amplitude of the topographic spectrum, h, in equation (3). For the wind-forced runs, however, the drag from this formulation was too low, and we empirically doubled the topographic height to $2h$. The reason for this difference will bear future scrutiny, but one possibility is that the stratification evolves differently in each type of simulation. In the wind-forced runs, any given parcel of topography sees low-frequency currents from different directions, and a continual input of dense water from the overturning circulation in the model. The body-forced runs, on the other hand, have flow always from one direction, meaning large-scale regions of blocked unstratified flow can develop over the duration of the simulations. This reduces the effective height of the topography (i.e. Aguilar and Sutherland 2006), and hence a reduced topographic height is accurate. This stagnant region may not have the ability to form in the eddying model, so the peak-to-peak amplitude of the topography is a more appropriate scale.

A related issue is that when we applied the drag law to the eddying simulations, we did not include the computational complexity of calculating the stratification, and instead used a constant N for the parameterization. This was just for convenience, and to see if the drag law was useful. However, given that the linear drag depends on N, this really should be done online, so that stratification is allowed to vary across the domain. Similarly, we would expect substantial mixing from the parameterized drag, but we have not included this extra mixing in the simulations used here; how this would feed back with the overturning circulation in the eddying simulations is an important question (Broadbridge et al. 2016). However, as noted, we did not run the models to thermal equilibrium, so testing this would require significantly more numerical expense.

An important caveat is that all the topography used here is stochastic, isotropic, and homogenous across the domain. These assumptions break down at the larger scales we are interested in, perhaps much more so than the smaller-scale "abyssal hills" that radiate lee waves. In particular, the effect of organized large-scale bathymetry, as opposed to stochastic bathymetry, should be investigated. Anisotropy may particularly matter if the different topographic wavelengths are organized in such a way as to be random for one direction, and in-phase for others.

Finally, the eddying simulations were somewhat cheaply run, and there is good evidence that changing the horizontal and vertical resolution can affect the near-bottom drag significantly in the presence of rough bathymetry (Klymak 2018). Our coarse ($\sim$40-m) vertical resolution also hampered our ability to look at smaller topographic amplitudes.

The overall importance of parameterizing the drag with an Nh/u_0-dependent hybrid between a linear drag and a quadratic one can be investigated by considering the bathymetry roughness parameterization as supplied by (Goff and Arbic 2010) and the global ocean data base of near-bottom stratification (FIG. 10). It is hard to compare the drag coefficients because they have very different magnitudes, though the linear drag co-efficient can be seen to be large at many locations in the ocean. If we choose a moderate eddying velocity of $U = 0.08$ m s^{-1}, then we can directly compare the drags produced in such a map. Overall, the quadratic drag dominates in most locations, but the regions where the quadratic drag is highest tend to be regions where the fraction of the total drag from the linear drag becomes more than 50% (FIG. 10f), indicating that including the linear drag for high-Nh/u_0 flows is valuable.

The scheme presented here benefits from substantial simplicity while retaining a Nh/u_0 dependence on the cross-over between the linear drag regime and the quadratic. To our knowledge, simulations have either used the linear or quadratic drag laws exclusively, and not used this hybrid approach. The lee-wave parameterizations (i.e. Nikurashin et al. 2014) work out to be linear drag laws, and the parameterizations that in addition account for non-propagating effects (Trossman et al. 2013, 2016) also are implemented as a linear drag with a geometric amplification. Conversely, non-propagating drag in the atmosphere is typically parameterized as a quadratic drag (Lott and Miller 1997; Scinocca and McFarlane 2000). Certainly, there are values of Nh/U that are large enough in the atmosphere to mean that the linear part of the drag law suggested here is important.
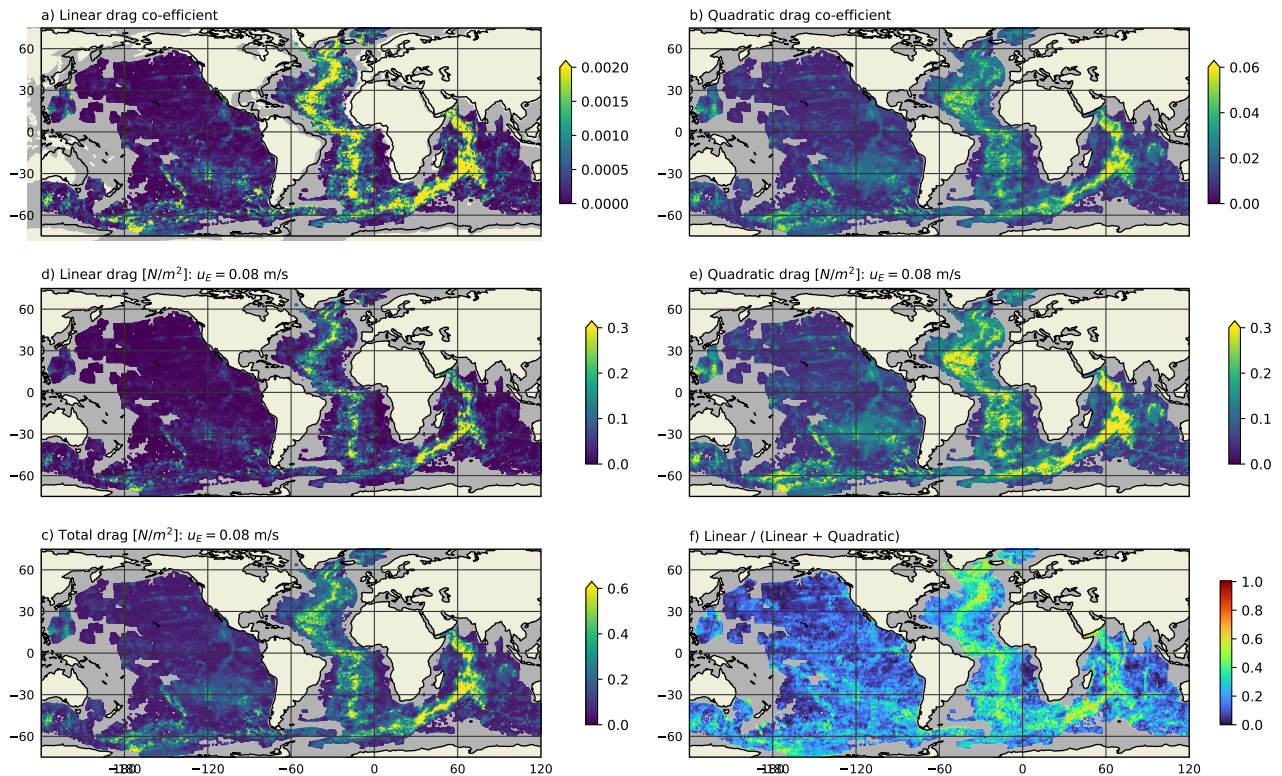
FIG. 10. Drag co-efficients proposed in this paper

References

Abernathey, R., and P. Cessi, 2014: Topographic enhancement of eddy efficiency in baroclinic equilibration. *J. Phys. Oceanogr.*, **44 (8)**, 2107–2126, doi:10.1175/jpo-d-14-0014.1.

Aguilar, D., and B. Sutherland, 2006: Internal wave generation from rough topography. *Physics of Fluids*, **18 (6)**, 066 603.

Bacmeister, J., and R. Pierrehumbert, 1988: On high-drag states of nonlinear stratified flow over an obstacle. *J. Atmos. Sci.*, **45 (1)**, 63–80.

Bell, T. H., 1975: Topographically generated internal waves in the open ocean. *J. Geophys. Res.*, **80 (3)**, 320–327.

Broadbridge, M. B., A. C. Naveira Garabato, and A. J. G. Nurser, 2016: Forcing of the overturning circulation across a circumpolar channel by internal wave breaking. *Journal of Geophysical Research: Oceans*, **121 (8)**, 5436–5451, doi:10.1002/2015jc011597, URL http://dx.doi.org/10.1002/2015JC011597.

Buijsman, M. C., and Coauthors, 2014: Three-dimensional double-ridge internal tide resonance in Luzon Strait. *J. Phys. Oceanogr.*, **44 (3)**, 850–869, doi:10.1175/JPO-D-13-024.1.

de Lavergne, C., G. Madec, F. Roquet, R. M. Holmes, and T. J. McDougall, 2017: Abyssal ocean overturning shaped by seafloor distribution. *Nature*, **551 (7679)**, 181–186, doi:10.1038/nature24472, URL http://dx.doi.org/10.1038/nature24472.

Garner, S. T., 2005: A topographic drag closure built on an analytical base flux. *J. Atmos. Sci.*, **62 (7)**, 2302–2315, doi:10.1175/jas3496.1.

Goff, J. A., and B. K. Arbic, 2010: Global prediction of abyssal hill roughness statistics for use in ocean models from digital maps of paleo-spreading rate, paleo-ridge orientation, and sediment thickness. *Ocean Modelling*, **32 (1-2)**, 36–43, doi:10.1016/j.ocemod.2009.10.001, URL http://dx.doi.org/10.1016/j.ocemod.2009.10.001.

Klymak, J. M., 2018: Nonpropagating form drag and turbulence due to stratified flow over large-scale abyssal hill topography. *J. Phys. Oceanogr.*, **48 (10)**, 2383–2395, doi:10.1175/jpo-d-17-0225.1, URL http://dx.doi.org/10.1175/JPO-D-17-0225.1.

Klymak, J. M., S. Legg, and R. Pinkel, 2010: High-mode stationary waves in stratified flow over large obstacles. *J. Fluid Mech.*, **644**, 312–336, doi:10.1017/S0022112009992503.

Klymak, J. M., and S. M. Legg, 2010: A simple mixing scheme for models that resolve breaking internal waves. *Ocean Modell.*, **33 (3-4)**, 224 – 234, doi:10.1016/j.ocemod.2010.02.005.

Klymak, J. M., H. L. Simmons, D. Braznikov, S. Kelly, J. A. MacKinnon, M. H. Alford, R. Pinkel, and J. D. Nash, 2016: Reflection of linear internal tides from realistic topography: The Tasman continental slope. *J. Phys. Oceanogr.*, doi:10. 1175/jpo-d-16-0061.1.

Lott, F., and M. J. Miller, 1997: A new subgrid-scale orographic drag parametrization: Its formulation and testing. *Quarterly Journal of the Royal Meteorological Society*, **123 (537)**, 101–127, doi:10.1002/qj.49712353704.

Marshall, D. P., M. H. P. Ambaum, J. R. Maddison, D. R. Munday, and L. Novak, 2017: Eddy saturation and frictional control of the Antarctic Circumpolar Current. *Geophys. Res. Lett.*, **44 (1)**, 286–292, doi: 10.1002/2016gl071702, URL http://dx.doi.org/10.1002/ 2016GL071702.

Marshall, J., A. Adcroft, C. Hill, L. Perelman, and C. Heisey, 1997: A finite-volume, incompressible Navier-Stokes model for studies of the ocean on parallel computers. *J. Geophys. Res.*, **102 (C3)**, 5753–5766, doi:10.1029/96JC02775.

Melet, A., R. Hallberg, S. Legg, and K. Polzin, 2013: Sensitivity of the ocean state to the vertical distribution of internal-tide-driven mixing. *J. Phys. Oceanogr.*, **43 (3)**, 602–615, doi:10.1175/JPO-D-12-055.1.

Munday, D. R., H. L. Johnson, and D. P. Marshall, 2015: The role of ocean gateways in the dynamics and sensitivity to wind stress of the early antarctic circumpolar current. *Paleoceanography*, **30 (3)**, 284–302, doi:10.1002/2014pa002675, URL http://dx.doi.org/10.1002/2014PA002675.

Nikurashin, M., and R. Ferrari, 2010: Radiation and dissipation of internal waves generated by geostrophic motions impinging on small-scale topography: Theory. *Journal of Physical Oceanography*, **40 (5)**, 1055–1074.

Nikurashin, M., R. Ferrari, N. Grisouard, and K. Polzin, 2014: The impact of finite-amplitude bottom topography on internal wave generation in the southern ocean. *J. Phys. Oceanogr.*, **44 (11)**, 2938–2950, doi:10.1175/ JPO-D-13-0201.1.

Polzin, K. L., 2009: An abyssal recipe. *Ocean Modelling*, **30 (4)**, 298–309, doi:10.1016/j.ocemod.2009.07.007.

Scinocca, J. F., and N. A. McFarlane, 2000: The parametrization of drag induced by stratified flow over anisotropic orography. *Quarterly Journal of the Royal Meteorological Society*, **126 (568)**, 2353–2393, doi:10.1002/qj.49712656802.

Shakespeare, C. J., and A. M. Hogg, 2017: The viscous lee wave problem and its implications for ocean modelling. *Ocean Modelling*, **113**, 22–29, doi:10.1016/j.ocemod.2017. 03.006, URL http://dx.doi.org/10.1016/j.ocemod.2017.03. 006.

Thompson, A. F., and A. C. Naveira Garabato, 2014: Equilibration of the antarctic circumpolar current by standing meanders. *Journal of Physical Oceanography*, **44 (7)**, 1811–1828, doi:10.1175/jpo-d-13-0163.1, URL http://dx. doi.org/10.1175/JPO-D-13-0163.1.

Trossman, D. S., B. K. Arbic, S. T. Garner, J. A. Goff, S. R. Jayne, E. J. Metzger, and A. J. Wallcraft, 2013: Impact of parameterized lee wave drag on the energy budget of an eddying global ocean model. *Ocean Modell.*, **72**, 119–142, doi:10.1016/j.ocemod.2013.08.006.

Trossman, D. S., B. K. Arbic, J. G. Richman, S. T. Garner, S. R. Jayne, and A. J. Wallcraft, 2016: Impact of topographic internal lee wave drag on an eddying global ocean model. *Ocean Modell.*, **97**, 109–128, doi:10.1016/j.ocemod. 2015.10.013.

Trossman, D. S., S. Waterman, K. L. Polzin, B. K. Arbic, S. T. Garner, A. C. Naveira-Garabato, and K. L. Sheen, 2015: Internal lee wave closures: Parameter sensitivity and comparison to observations. *Journal of Geophysical Research: Oceans*, **120 (12)**, 7997–8019, doi:10.1002/2015jc010892, URL http://dx.doi.org/10.1002/2015JC010892.